ELSEVIER

Journal of Alloys and Compounds 408–412 (2006) 266–272

Journal of ALLOYS AND COMPOUNDS

www.elsevier.com/locate/jallcom

Metastable phase formation from undercooled melt of Nd–Fe–B alloys

Kazuhiko Kuribayashi *, Shumpei Ozawa

Institute of Space and Astronautical Science, Japan Aerospace Exploration Agency, 3-1-1, Yoshinodai, Sagamihara, Kanagawa 229-8510, Japan

Available online 13 June 2005

Abstract

The undercooled melts of the Nd–Fe–B alloy, the chemical composition of which is stoichiometric $Nd_2Fe_{14}B$, solidified during free fall in a 26 m drop tube. The microstructures of the as-dropped samples were examined using X-ray diffraction analyzer and a scanning electron microscope with an energy dispersive X-ray analyzer. The microstructures were classified into two types: type I is the mixture of properitectic α-Fe and peritectic $Nd_2Fe_{14}B$, and type II is the monochromatic metastable phase having a crystal structure similar to that of rhombohedral Nd_2Fe_{17}. The samples cooled at relatively low cooling rates were observed to be type I and the samples cooled at relatively high cooling rates were observed to be type II. The high cooling rate followed by high undercooling facilitates the formation of the metastable phase directly in the undercooled melt. The critical conditions for the formation of the metastable phases in the undercooled melt are thermodynamically and kinetically discussed.

Keywords: Nd–Fe–B alloy; Metastable phase; Undercooling; Containerless processing; Drop tube

1. Introduction

It is well known that the superiority of Nd–Fe–B magnets results from the intermetallic $Nd_2Fe_{14}B$ hard magnetic phase, which is formed via a peritectic reaction between the properitectic Fe phase and the liquid phase. In the cast Nd–Fe–B alloy, however, the properitectic Fe phase, the morphology of which is usually dendritic, remains undissolved. The reason is that the rate of the peritectic reaction is controlled by the solid-state diffusion of Fe in the precipitated $Nd_2Fe_{14}B$ phase. As an attempt to form Nd–Fe–B alloy free of the α-Fe, the direct crystallization of the $Nd_2Fe_{14}B$ phase from the undercooled melts is carried out by containerless processing, such as electromagnetic levitation or free falling in a drop tube. In these studies [1–4], it has been expected that rapid solidification into the undercooled melt can reduce the amount of α-Fe. The experimental results, however, showed that the metastable $Nd_2Fe_{17}B_x$ phase was formed instead of the $Nd_2Fe_{14}B$ phase.

If melts are undercooled to far below the equilibrium melting temperature, various solidification pathways occur, such as crystallization to stable and metastable phases, quasi-crystallization and vitrification. Since vitrification is a phenomenon indicating deviation far from the equilibrium state, the thermodynamic and kinetic conditions are very simple, that is, merely to cool the melt rapidly in order that the critical nucleus may not be formed. In the case of the crystallization of metastable phases, however, the thermodynamic and kinetic conditions are complex. There must be critical control of the undercooling level and cooling rate. In the present study, using Nd–Fe–B alloys as a model material, the critical condition for the forming of metastable phases was studied from the thermodynamic and kinetic points of view.

2. Experimental

In the present study, the stoichiometric $Nd_2Fe_{14}B$ alloy whose chemical composition is $Nd_{11.8}Fe_{82.3}B_{5.9}$ was used as the model material. High-purity elemental materials (Nd 99.9%, Fe 99.99% and B 99.8%) were alloyed to form a

* Corresponding author.
E-mail address: kuribayashi@isas.jaxa.jp (K. Kuribayashi).

0925-8388/$ – see front matter © 2005 Elsevier B.V. All rights reserved.
doi:10.1016/j.jallcom.2005.04.058

source ingot using an inductive melting furnace in an atmosphere of inert gas. The source ingot, after being cut into small pieces, was cleaned acoustically in acetone and then placed in a quartz crucible with an orifice from 0.1 to 0.5 mm in diameter at the bottom. The quartz crucible was set in the vacuum chamber mounted at the top of the drop tube. Fig. 1 shows schematic drawing of the drop tube used in the present experiment, the free fall length of which is 26 m [2]. The drop tube was initially evacuated to 1×10^{-4} Pa and then backfilled with either Ar or He of 99.9995% purity, which were used for changing the cooling rate of falling droplets, that is, Ar was used for achieving a relatively low cooling rate and He vice versa. The source ingot was inductively heated to 1650 K and held for 5 s at this temperature, to ensure it to be completely melted. The temperature of the melt was monitored at the center of the crucible with a thermocouple sheathed in quartz glass. Then, the melt was ejected into the drop tube through the orifice by controlling the gas pressure in the crucible. The samples collected at the bottom of the drop tube were classified into several groups according to their diameters, which ranged from 300 to 1500 μm. The shape of the as-dropped samples was almost spherical. This means the samples solidified without touching the container wall that has a strong catalytic potential for inducing heterogeneous nucleation. In addition, the decrease in the number of potential nucleation sites in a droplet with decreasing diameter is also favorable for enhancement of the undercooling level.

The bulk composition of the as-dropped samples was analyzed by inductively coupled plasma atomic emission spectrometry (ICP-AES). The constituent phases of the samples were identified by powdered X-ray diffraction (XRD) analysis using Cu Kα radiation at room temperature. The microstructure of the samples was examined using a scanning electron microscope equipped with an energy dispersive spectra (SEM–EDS) analyzer.

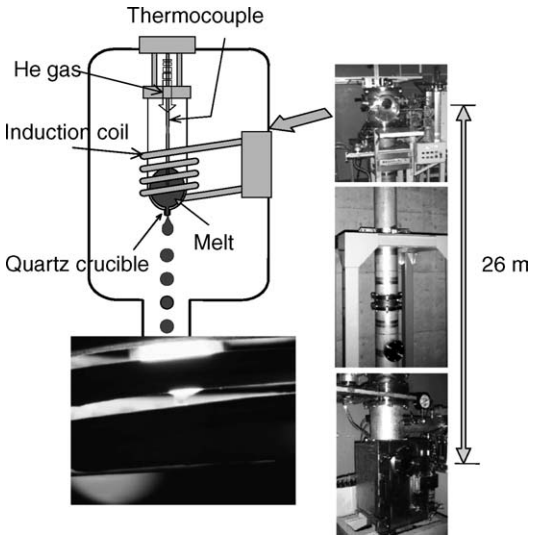

Fig. 1. Schematic illustration of drop tube used in present experiment.

3. Results

In spite of the high oxidization tendency of the Nd–Fe–B alloy in ambient air, the surface of the as-dropped samples exhibited a metallic luster. This means the droplets solidified in the oxygen-free atmosphere. Fig. 2 shows the XRD patterns of the as-dropped samples with various diameters in the range from 200 to 1200 μm, where (a–c) denote the samples dropped in the Ar atmosphere, and (d and e) denote the samples dropped in the He atmosphere. For comparison, the XRD pattern of the source ingot is also depicted. The XRD patterns of (a and b) agree well with that of the source ingot, for which the tetragonal $Nd_2Fe_{14}B$ phase and the α-Fe phase are well indexed. On the other hand (c–e), where the α-Fe phase is not clear, show the diffraction profiles indexed according to that of rhombohedral Nd_2Fe_{17}. Compared with the XRD pattern of the source ingot, a limited number of diffraction peaks are shown in the (c–e) profiles. This means that the lattice symmetry of the phase concerned is higher than that of the $Nd_2Fe_{14}B$ phase, being similar to the case of the metastable phase in rare earth ferrite formed from the highly undercooled melt [5].

Fig. 3(a–e) show the cross-sectional microstructures of the as-dropped samples with various diameters, where Fig. 3(a–c) show the samples dropped in Ar, and Fig. 3(d and e) show the samples dropped in He. As shown in Fig. 3(a), two types of precipitates were observed in the matrix; one is segmented dendrite embedded in the matrix grain, and the other is an intergranular precipitate. The EDS analysis reveals that the segmented dendrites and the intergranular precipitates are the α-Fe phase and the Nd-rich phase, respectively. It is evident that the α-Fe phase was formed via a solid-state transformation from the properitectic γ-Fe phase. The chem-

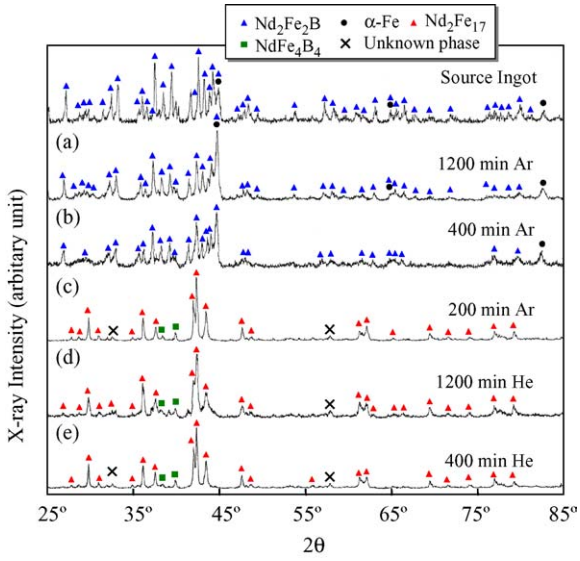

Fig. 2. XRD patterns of source ingot and as-dropped samples: (a) $d = 1200$ μm in Ar; (b) $d = 400$ μm in Ar; (c) $d = 200$ μm in Ar; (d) $d = 1200$ μm in He and (e) $d = 400$ μm in He.

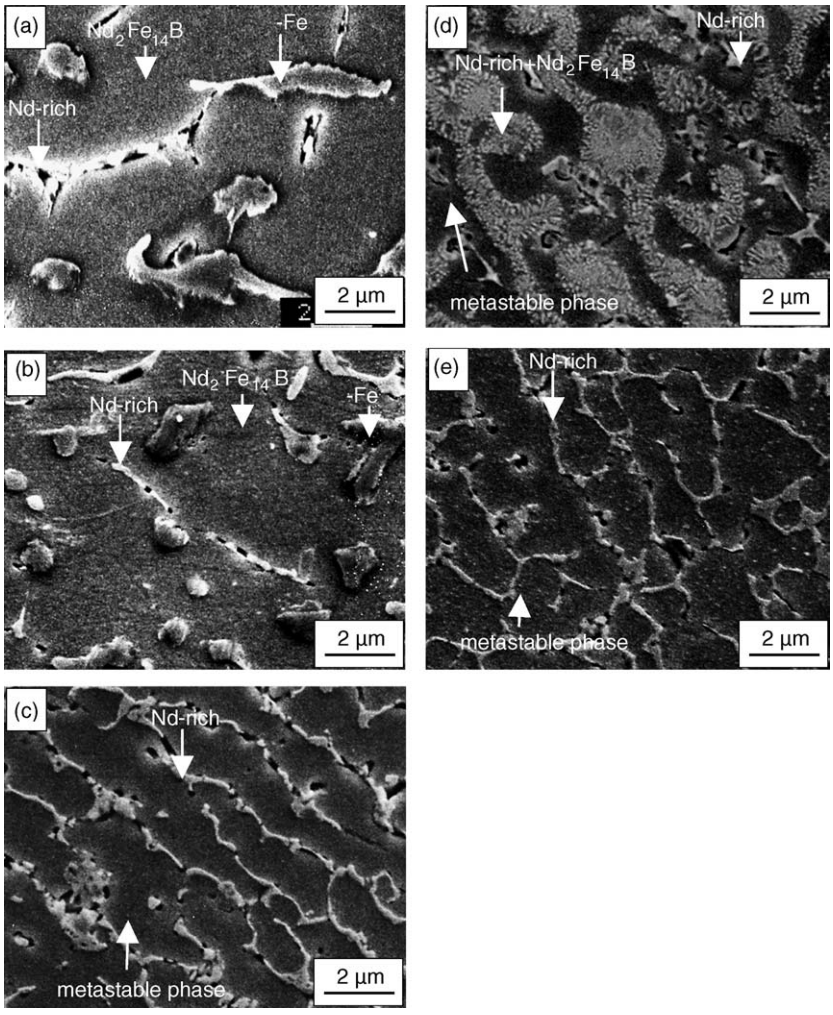

Fig. 3. Microstructures of as-dropped samples: (a) $d = 1200$ μm in Ar; (b) $d = 400$ μm in Ar; (c) $d = 200$ μm in Ar; (d) $d = 1200$ μm in He and (e) $d = 400$ μm in He.

ical composition of the matrix was nearly equal to that of the source ingot. With the help of the XRD analysis shown in Fig. 2, it is clear that the matrix is the $Nd_2Fe_{14}B$ phase. The phase constituent of the sample with a diameter of 400 μm dropped in Ar was almost the same as that of the sample with a diameter of 1200 μm, except that the grain size was more refined and the α-Fe dendrites were finely segmented. In the sample with a diameter of 200 μm, however, the phase constituency was clearly different from those of samples with diameters of 1200 and 400 μm. As shown in Fig. 3(c), there were no α-Fe dendrites in the matrix. These results, from the XRD and EDS analyses, indicate that the matrix of the sample with a diameter of 200 μm dropped in Ar was not the $Nd_2Fe_{14}B$ phase but the metastable phase that has the same crystal structure as that of Nd_2Fe_{17} and a chemical composition similar to that of the source ingot. This means that the increase in cooling rate due to the decrease in droplet diameter suppresses the nucleation of γ-Fe, and therefore, increases undercooling degree. Hence, deep undercooling was achieved and then the partitionless metastable phase with the crystal structure of $Nd_2Fe_{17}$was directly formed from the undercooled melt. On the basis of this presumption, it is expected that free falling in an atmosphere of He facilitates the formation of the metastable phase even in samples with relatively large diameters. As shown in Fig. 3(e), the microstructure of the sample with a diameter of 400 μm dropped in He is similar to that shown in Fig. 3(c), even though the sample diameter is twice as large as that of the sample shown in Fig. 3(c).

Summarizing these results, we have arrived at a preliminary conclusion, that is, the microstructures of the as-dropped Nd–Fe–B alloy can be classified into two types; type I is a mixture of properitectic α-Fe and peritectic $Nd_2Fe_{14}B$, and type II is a monochromatic metastable phase. In the sample with a diameter of 1200 μm dropped in He, however, the microstructure is neither type I nor type II. The microstructure shown in Fig. 3(d) consists of fine irregular lamellae of white and dark phases embedded in the column matrix, the morphology of which is similar to eutectoid structures such as “pearlite” in carbon steel. The average interlamellar spacing

is smaller than 1 μm. This indicates that the microstructure shown in Fig. 3(d) was formed by the solid-state reaction in the metastable phase during the postsolidification cooling stage.

4. Discussion

As mentioned in the previous section, the microstructures of the as-dropped samples were classified into two types: type I is the microstructure formed via the peritectic reaction between the properitectic γ-phase and the alloy melt, where the predominant phase is $Nd_2Fe_{14}B$, and type II the metastable phase free from α-Fe. The crystal structure of the metastable phase is that of Nd_2Fe_{17} and the chemical composition is similar to that of the source ingot. The type II microstructure is directly formed from the undercooled melt when the cooling rate of the falling droplet is sufficiently high for the properitectic γ-Fe phase not to be nucleated.

According to these experimental results, it is clear that the high cooling rate followed by high undercooling facilitates the direct formation of the metastable phase in the undercooled melt. In this section, then, we discuss the thermodynamics and kinetics of the metastable phase in the undercooled melt, and then extract the critical condition for the nucleation and growth of the metastable phases in the undercooled melts.

4.1. Free energy as a function of temperature for melt, metastable phase and stable phase

Fig. 4 shows the schematic drawings of the Gibbs free energy, G, as a function of temperature for the liquid phase, L, and two different solid states, S_1 and S_2, at a constant pressure [6]. According to the definition of the Gibbs free energy, the slope of the $G(T)$ curve corresponds to the entropy with a negative sign. If we express the entropy of the states as S_L, S_1 and S_2, the relationship $S_L > S_2 > S_1$ commonly exists in these states, where S_1, having a relatively low entropy, is stable at low temperatures, and S_2, having a relatively high entropy, becomes stable at high temperatures. In the high-temperature phase, the high entropy compared with that of the low-temperature phase results in a crystal structure that is disordered, and therefore, has a high symmetry. Hence, it can be easily understood that the entropy of fusion ΔS_f of S_2 is smaller than that of S_1.

If the $G(T)$ curve of S_2 moves upward as shown in Fig. 4(b) under the condition that S_2 is invariant, the temperature of the phase transformation from S_1 to S_2, T_{tr}, moves toward the equilibrium melting temperature, T_E. If T_{tr} becomes higher than T_E, the S_2 phase disappears in the equilibrium phase diagram. In the undercooled melt, however, the S_2 phase can be formed as a metastable phase, provided that the thermodynamic and kinetic conditions for the metastable phase to be nucleated and grown are satisfied.

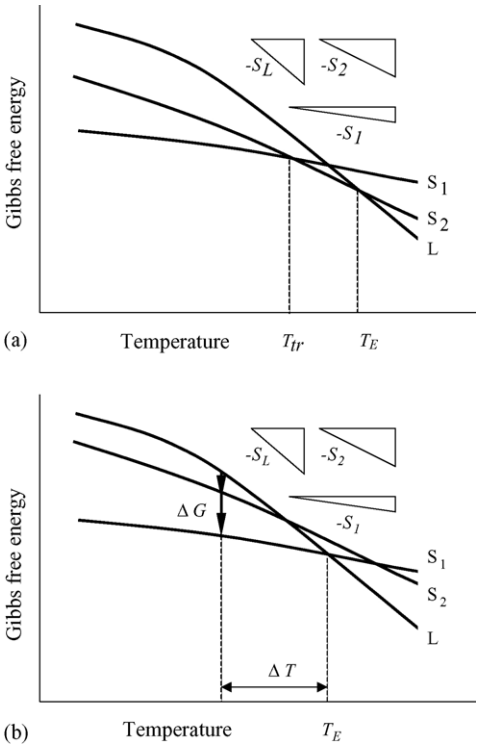

Fig. 4. Gibbs free energy G as function of temperature for liquid L and two different solid states S_1 and S_2 at constant pressure: (a) case in which S_2 intersects with S_1 at T_{tr} below equilibrium melting temperature; (b) case in which S_2 does not intersect with S_1.

4.2. Thermodynamic condition for metastable phase to nucleate

According to classical nucleation theory [7], the activation energy required for the formation of a critical nucleus, ΔG^*, is given by:

$$\Delta G^* = \frac{16\pi\sigma^3 f(\theta)}{3\Delta G^2} \quad (1)$$

where σ is the interface energy, $f(\theta)$ the contact angle function showing the catalytic potency for heterogeneous nucleation and ΔG is the Gibbs free-energy difference between the liquid and solid phases. Assuming the simplest approximation of ΔG, such as $\Delta G = \Delta S_f \Delta T$, an equivalent $f(\theta)$ for stable and metastable phases, and the negentropic model of the interface energy, that is, $\sigma = \alpha \Delta S_f T / N^{1/3} V_m{}^{2/3}$ [8], Eq. (1) is rewritten as:

$$\Delta G^* = \frac{16\pi\alpha^3 \Delta S_f T^3}{3 N V_m^2 \Delta T^2} \quad (2)$$

where ΔT is undercooling expressed by $T_E - T$, N Avogadro's number and V_m is the molar volume. The scaling factor α, which depends on the crystal structure of the nucleus, was calculated as 0.86 in the cases of fcc and hcp structures, and 0.71 in the case of the bcc structure [8]. Furthermore, α was experimentally estimated to be approximately 0.5 for semiconductive silicon [9].

The negentropic model of the interface energy, which enables the temperature dependence of the interface energy to be incorporated into Eq. (1), has been applied in the phase selection between δ-and γ-phases in binary Fe–Ni [10] and ternary Fe–Ni–Cr [11] solid solutions. For solids having a complicated crystal structure such as $Nd_2Fe_{14}B$, however, the scaling factor has not been determined. Holland-Moritz [12], however, showed using structural models of the interfaces of several Al–transition metal compounds, that the scaling factor for polytetrahedrally packed structures should be less than that for pure metals, being minimum for quasi-crystalline compounds. Some typical values are 0.43 for Al_5Fe_2, 0.39 for $Al_{13}Fe_4$ and 0.34 for the icosahedral phase. On the basis of his results, we assume the value of α to be 0.5, which is the intermediate value between pure metals and quasi-crystalline compounds. In that case, the phase selection between the stable and metastable phases at the nucleation stage, which is controlled by the entropy of fusion, can be formulated.

Fig. 5 shows the critical undercooling, ΔT_c^n, as a function of the entropy of fusion of the metastable phase, ΔS_f^{ms}, where ΔT_c^n and ΔS_f^{ms} are normalized with T_E^s and ΔS_f^s, respectively. The superscripts, s and ms, indicate the stable phase and the metastable phase, respectively. Concerning the hypothetical melting temperature of the metastable phase, two cases are shown: one shown by the bold line is when T_E^{ms} is assumed to be $0.95T_E^s$, and the other shown by the dashed line is when it is assumed to be $0.98T_E^s$. The curves are the lines along which $\Delta G^{*s} = \Delta G^{*ms}$. On the left-hand sides of the curves, where $\Delta G^{*s} > \Delta G^{*ms}$, the metastable phase nucleates dominantly, while the stable phase is dominant on the right-hand sides of the curves, where $\Delta G^{*s} < \Delta G^{*ms}$. This figure clearly shows that the critical factor in phase selection at the nucleation stage is the entropy of fusion of the metastable phase. The smaller entropy of fusion facilitates the metastable phase to nucleate more preferentially even with less extreme undercooling.

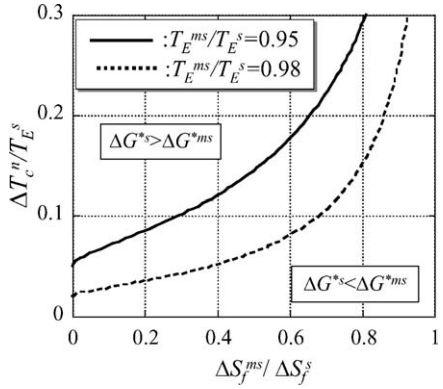

Fig. 5. Relationship between critical undercooling ΔT_c^n, above which activation energy required for formation of critical nucleus of metastable phase exceeds that of stable phase, and entropy of fusion of metastable phase ΔS_f^{ms}. ΔT_c^n and ΔS_f^{ms} are normalized using T_E^s and ΔS_f^s, respectively.

4.3. Kinetic condition for metastable phases to grow

Under the assumption of diffusion-limited crystal growth, the growth velocity V is given by the difference between the rates of attachment and detachment of growth units at a growth front:

$$V = a\nu \exp\left(-\frac{\Delta S_f}{k_B}\right) \exp\left(-\frac{E_D}{k_B T}\right) \left[1 - \exp\left(-\frac{\Delta G}{k_B T}\right)\right] \quad (3)$$

where a, ν and E_D are the interatomic distance, the atomic vibration frequency and the activation energy for atomic diffusion in the liquid phase. The first exponential function is due to the difference in the numbers of states between the solid and liquid phases, that is, $\exp(-\Delta S_f/k_B) = W_s/W_l$ [13], where W_s and W_l are the numbers of states in the solid and the liquid phases, respectively.

If ΔG can be assumed to be sufficiently small for the higher-order term in the series expansion of the exponential function in the bracket to be ignored, a kinetic coefficient $\mu = V/\Delta T_k$ is given by:

$$\mu = \frac{D}{aT} \frac{\Delta S_f}{k_B} \exp\left(-\frac{\Delta S_f}{k_B}\right) \quad (4)$$

where ΔT_k denotes kinetic undercooling at an interface and D is the diffusion coefficient in the liquid phase. Fig. 6 shows the relationship between the kinetic coefficient and the dimensionless entropy of fusion $\Delta S_f/k_B$. As shown in this figure, the kinetic coefficient passes through a maximum at $\Delta S_f/k_B = 1$. In close-packed metals such as Cu and Ni, the entropy of fusion has been reported as approximately 1.0–1.2 k_B [14], which is the minimum in normal metals. In this case, metastable phases having kinetic coefficients larger than those of stable phases are never anticipated. In intermetallic compounds and semiconductive materials, however, $\Delta S_f/k_B$ is much larger than 1, where metastable phases whose kinetic coefficients are intermediate may be discovered.

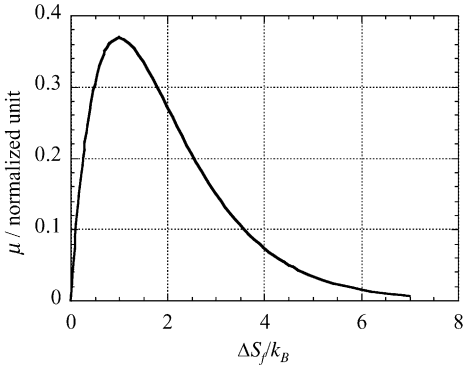

Fig. 6. Relationship between kinetic coefficient μ and dimensionless entropy of fusion $\Delta S_f/k_B$.

4.4. Crystal growth velocities in stable and metastable phases as function of undercooling

In the case of the solidification into undercooled melts, the bulk undercooling ΔT is given by:

$$\Delta T = \Delta T_t + \Delta T_r + \Delta T_s + \Delta T_k \quad (5)$$

where ΔT_t is the thermal undercooling given by:

$$\Delta T_t = \frac{\Delta H_f}{C_P} \mathrm{Iv}(P_t) \quad (6)$$

for the case in which the shape of the growth front can be approximated using an elliptical paraboloid. In this equation, ΔH_f is the enthalpy of fusion, C_P is the specific heat of the melt at constant pressure, and Iv(Pt) is the Ivantsov function [15] given by:

$$\mathrm{Iv}(P_t) = P_t \exp(P_t) \int_{P_t}^{\infty} \frac{\exp(-P_t)}{P_t} \mathrm{d}P_t \quad (7)$$

where $P_t = VR/2a_l$ denotes the thermal Peclet number, R the radius of the growth front and a_l the thermal diffusivity.

In Eq. (5), the curvature undercooling due to the Gibbs–Thomson effect, ΔT_r, is expressed by:

$$\Delta T_r = \frac{2\Gamma}{R} \quad (8)$$

where $\Gamma = \sigma/\Delta S_f$ is the Gibbs–Thomson coefficient. In an alloy system with a solute distribution, the constitutional undercooling ΔT_s must be taken into account. In the present experiment, however, the chemical composition of the material used is stoichiometric $Nd_2Fe_{14}B$, and partitionless crystallization is assumed regardless of the crystallized phase, stable or metastable. Therefore, ΔT_s can be ignored.

As stated above, the kinetic undercooling ΔT_k is given by:

$$\Delta T_k = \frac{V}{\mu} \quad (9)$$

According to the marginal stability analysis [16], the radius of the growth front that is assumed to be equal to the wavelength of a critical perturbation of a planar interface λ_I is derived as:

$$R = \frac{\Gamma/\sigma^*}{P_t \frac{\Delta H_f}{C_P} \left(1 - \frac{1}{\sqrt{\sigma^* P_t^2}}\right)}, \quad (10)$$

where σ^*, a stability constant, was approximately derived to be 0.025 using the marginal stability criterion [17].

Using Eqs. (5)–(10), and the negentropic model of the interface energy, we calculated the relation between growth velocities and undercooling under the condition of low undercooling. Fig. 7(a and b) show the results, where Fig. 7(a) shows the case in which T_E^{ms} is assumed to be $0.98T_E^s$ and Fig. 7(b) shows the case in which T_E^{ms} is assumed to be $0.95T_E^s$. The typical values for the physical properties of the model material assumed in the calculation are listed in Table 1. The entropies of fusion of the stable and metastable

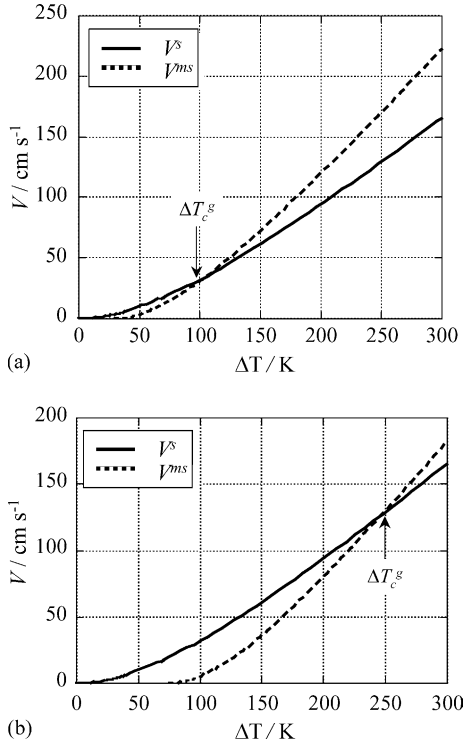

Fig. 7. Relationship between growth rates V and undercooling ΔT calculated under assumption that entropies of fusion of stable and metastable phases are 2 and 1.2 k_B, respectively: (a) case that T_E^{ms} is assumed to be $0.98T_E^s$, and (b) case that T_E^{ms} is assumed to be $0.95T_E^s$. ΔT_c^g denotes critical undercooling, above which growth velocity of metastable phase exceeds that of stable phase.

phases are assumed to be 2.0 and 1.2 k_B, respectively. Therefore, the kinetic coefficient, μ, of the growth of the metastable phase is calculated to be 1.33 times larger than that of the stable phase. The slope of V versus ΔT for the metastable phase is similar to that of the stable phase. The arrows denote the critical undercooling ΔT_c^g, above which the growth velocity of the metastable phase exceeds that of the stable phase. Comparing Fig. 7(b) with (a), it looks as if the change in T_E^{ms} merely shifts the curve towards the high-undercooling side. The change in ΔT_c^g due to the translation, however, is larger than the translation, being several times larger than the change in T_E^{ms}. It is clear that T_E^{ms}, in particular the ratio T_E^{ms}/T_E^s, strongly affects ΔT_c^g. Furthermore, it is noteworthy that ΔT_c^g is almost the same as ΔT_c^n shown in Fig. 2. This means that the critical condition for the nucleation of the metastable phase simultaneously satisfies the growth condition of the

Table 1
Material parameters used in calculation

Parameter	Dimension	
C_p/k_B	3.5	
T_E^s	K	1500
a_l	$cm^2\ s^{-1}$	0.05
D	$cm^2\ s^{-1}$	1×10^4
V_m	$cm^3\ mol^{-1}$	8
a	cm	2×10^{-8}

metastable phase. The situation is similar for the case in which $\Delta S_f^{ms}/\Delta S_f^{s}$ is 0.3. In these cases, the metastable phase can be frozen at room temperature if the postsolidification cooling rate is sufficiently high for the solid-state diffusional transformation to the stable phase to be suppressed, as in the case of free falling in the drop tube. In Fe–Ni [10] and Fe–Ni–Cr [11] alloys with the chemical composition in which fcc γ is the stable phase, the bcc δ phase has never been frozen despite the fact that undercooling the melt below the critical temperature promotes the nucleation of the bcc δ phase. This is because the dimensionless entropies of fusion of bcc δ and fcc γ are approximately 1, at which the growth velocity of a stable phase is always faster than that of a metastable phase. It is clear that the critical factor in phase selection is the ratio of ΔS_f^{ms} to ΔS_f^{s}. If the value is small, for example 0.5, the metastable phase nucleates and grows under an intermediate level of undercooling.

5. Conclusion

Using the Nd–Fe–B alloy whose chemical composition was stoichiometric $Nd_2Fe_{14}B$ as the model material, containerless solidification processing was carried out in a 26 m drop tube. The microstructures of the as-dropped samples were investigated, and were classified into two types depending on their diameters; type I, that was observed for relatively large samples, is the microstructure formed via the peritectic reaction between the properitectic γ-phase and the alloy melt, where the predominant phase is $Nd_2Fe_{14}B$, and type II, that was observed for relatively small samples, is the predominant metastable phase free of α-Fe. The crystal structure of the metastable phase is that of Nd_2Fe_{17} and its chemical composition is similar to that of the source ingot. The type II microstructure is directly formed from the undercooled melt when the cooling rate of the falling droplet is sufficiently high for the properitectic γ-Fe phase not to be nucleated. On the basis of the thermodynamics and kinetics of nucleation and growth, we have arrived at the conclusion that the critical factor in phase selection between stable and metastable phases is the ratio of the entropy of fusion of a metastable phase to that of a stable phase. If the ratio is small, typically less than 0.6, the critical condition for the nucleation of the metastable phase can simultaneously satisfy the growth condition of the metastable phase. For example, moderate undercooling, such as 7% of the equilibrium melting temperature, will be sufficient for the metastable phase to preferentially nucleate and subsequently grow faster than the stable phase, provided that the difference between the equilibrium melting temperature of the stable phase and the hypothetical melting temperature of the metastable phase is as small as 2% of the equilibrium melting temperature of the stable phase.

Acknowledgements

This work was financially supported by a grant in aid for Scientific Research from the Ministry of Education, Culture, Sports, Science and Technology. One of the authors (SO) acknowledges the Japan Society for Promotion of Science (JSPS) for the offer of a JSPS fellowship.

References

[1] J. Gao, T. Volkmann, D.M. Herlach, Acta Mater. 50 (2003) 3003–3012.
[2] S. Ozawa, M. Li, K. Kuribayashi, Mater. Trans. 44 (2003) 806–810.
[3] S. Ozawa, M. Li, K. Kuribayashi, S. Sugiyama, I. Jimbo, S. Hirosawa, J. Appl. Phys. 95 (2004) 8478–8480.
[4] S. Ozawa, M. Li, S. Sugiyama, I. Jimbo, K. Kuribayashi, Mater. Sci. Eng. A 382 (2004) 295–300.
[5] K. Nagashio, K. Kuribayashi, J. Am. Ceram. Soc. 85 (2002) 2550–2556.
[6] D.M. Herlach, Mater. Sci. Eng. R12 (1994) 117–265.
[7] K.F. Kelton, Solid State Phys. 45 (1991) 75–177.
[8] C.V. Thompson, F. Speapen, Acta Metal. 31 (1983) 2021–2027.
[9] T. Aoyama, Y. Takamura, K. Kuribayashi, Jpn. J. Appl. Phys. 37 (1998) L687–L690.
[10] D.J. Thoma, J.H. Perepezko, Metall. Trans. A 23A (1992) 1347–1362.
[11] W. Loeser, D.M. Herlach, Metall. Mater. Trans. A 23A (1992) 1585–1591.
[12] D. Holland-Moritz, Int. J. Non-Equilib. Process. 11 (1998) 169–199.
[13] Y. Saito, Statistical Physics of Crystal Growth, World Scientific, Singapore, 1996.
[14] W.F. Gale, T.C. Totemeier (Eds.), Smithells Metals Reference Book, eighth ed., Elsevier, 2004.
[15] G.P. Ivantsov, Dokl. Akad. Nauk SSSR 58 (1947) 567–569.
[16] W. Kurz, D.J. Fisher, Acta Metall. 29 (1981) 11–20.
[17] J. Lipton, W. Kurz, R. Trivedi, Acta Metall. 35 (1987) 957–964.